Real-space TB-LMTO spin-polarized self-consistent calculations of the electronic structure of the amorphous alloys Ni-B, Fe-B and Zr-Be

1993 J. Phys.: Condens. Matter 5 3203

(http://iopscience.iop.org/0953-8984/5/19/018)

J. Phys.: Condens. Matter 5 (1993) 3203–3220. Printed in the UK

Real-space TB-LMTO spin-polarized self-consistent calculations of the electronic structure of the amorphous alloys Ni–B, Fe–B and Zr–Be

A M Bratkovsky†§ and A V Smirnov‡

† Research Centre in Superconductivity, University of Cambridge, Cambridge CB3 0HE, UK
‡ Computer Centre, Kurchatov Institute, 123182 Moscow, Russia

Received 17 November 1992, in final form 16 March 1993

Abstract. The first-principles tight-binding (TB)-LMTO method is used for self-consistent calculations of the electronic structure of the amorphous $Fe_{80}B_{20}$, $Ni_{100-x}B_x$ and Zr_xBe_{100-x} alloys in combination with the recursion method. Realistic structure models were constructed with the use of the Monte Carlo method. The electron density has been calculated self-consistently for the given amorphous structures.

We describe our results for the electronic structure of amorphous $Fe_{80}B_{20}$, which is a typical transition-metal–metalloid glass. In the paramagnetic phase it has a generic double-peak structure close to the Fermi level formed by non-bonding Fe d orbitals, with a bonding B p–Fe d hybrid at lower energies, in agreement with previous calculations. We present the spin-polarized LSDA calculations, which show that the d band splits, resulting in a strong itinerant magnetism in $Fe_{80}B_{20}$ with a net moment on Fe atoms of $\bar{\mu} = 2.14\mu_B$, in good agreement with experiment and estimated values from generalized Stoner criteria. The DOS in a-$Ni_{100-x}B_x$ has a shape similar to that of paramagnetic $Fe_{80}B_{20}$ shifted downwards from the Fermi level, which explains the paramagnetic behaviour of all studied Ni-based glasses (x=20, 25 and 34). With increasing B content the height of the main DOS peak formed by the Ni d electrons decreases and the strength of the covalent Ni d–B p interaction increases. In Ni-rich glasses the onset of ferromagnetism corresponds to a B concentration below some threshold and the present LSDA calculations predict a net moment $\bar{\mu} = 0.43\mu_B$ in pure a-Ni. Comparison of the DOS with photoemission data indicates that the calculated Ni d band in $Ni_{80}B_{20}$ is shifted downwards by 0.25 eV and broadened by 1.1 eV as a result of the local density approximation, where non-locality and dynamic correlations are lacking.

The calculated DOS in a-Zr_xBe_{100-x} is dominated by the broad Zr d band. In all studied glasses a significant hybridization between transition metal d and metalloid/simple-metal p states takes place.

By making use of low-temperature heat capacity and magnetic susceptibility data for Ni–B and Zr–Be glasses we show a good agreement with the calculated DOS at the Fermi level, $N(0)$, if electron–phonon and exchange enhancements are taken into account.

1. Introduction

The purpose of the present work is to study the electronic structure of the transition-metal–metalloid (Ni–B, Fe–B) and transition-metal–simple-metal (Zr–Be) glasses with *ab initio* density functional theory. The results of the present study as regards the trends in the electron density of states, etc, are likely to be generic for the classes of glassy metals with similar bonding.

§ Email address: amb27@cus.cam.ac.uk

0953-8984/93/193203+18$07.50

The amorphous borides have been extensively studied experimentally, revealing unique magnetic properties [1–5], Invar behaviour [6] and high mechanical properties. Perhaps remarkably, the properties of transition-metal–metalloid (TMM) crystalline compounds are quite similar to those of their amorphous counterparts with the same composition, for example as regards the electronic structure of Fe–B and Ni–B glasses studied by high-resolution UV photoemission, XPS, Auger electron and energy-loss spectroscopy [7, 8]. It has been known since the pioneering work of Kiessling [9] that covalent bonding in crystalline borides corresponding to B p orbitals is responsible for the complicated unit cell and other properties, but little is known about what happens to the B p–B p and B p–TM d bonds in an amorphous environment, i.e. what is the possible charge transfer between unlike atoms and its effect with respect to the crystalline counterpart. A comparative study of a system consisting of a transition metal and a simple sp metal would be interesting. It is almost obvious that sp–d bonds should not be strong there, but a quantitative picture is still lacking. We discuss below the electronic structure of the amorphous alloys $Fe_{80}B_{20}$, $Ni_{100-x}B_x$ and Zr_xBe_{100-x}.

The Fe–B glass is a classical amorphous system, which can be used as a reference system for comparison with other TMM glasses. The $Ni_{100-x}B_x$ glasses could be formed in a wide range of compositions, also covering systems with direct contact between metalloid atoms. In particular, in the $Ni_{66}B_{34}$ glass, the boron–boron coordination number $Z_{BB} \approx 1$ [10, 11], i.e. boron atoms are in direct contact, which is not the case in the crystalline counterpart and forbidden in the Polk model of 80:20 glasses [12, 13]. It is also an established fact that the magnetic moment of the Ni atoms is 'fragile', and disappears upon small dilution by non-magnetic atoms. This aspect of the electronic structure of amorphous nickel borides will also be addressed below. Amorphous Zr–Be is a new intermetallic glassy system, containing a transition metal and a simple metal with a large size and mass ratio. It results in an interesting atomic structure, and interesting dynamics and electronic properties, studied by low-temperature measurements [14].

The first-principles description of the electronic structure and properties of topologically disordered systems is a challenging problem in solid state research. The lack of translational symmetry represents the main obstacle to constructing a quantitative theory comparable in efficiency with those for crystalline solids based on the electron density functional method ([15] and references therein). The electronic structure and properties of transition metal amorphous alloys, which play an important role in applications, are believed to be defined mainly by the localized d electrons, hence it was customary to use the semi-empirical tight-binding (TB) Hamiltonians to describe the electronic properties. In spite of encouraging success in applying the semi-empirical TB Hamiltonians some underlying approximations often remain unjustified, such as the implementation of the method to the extended s- and p-electron states, the transferability of parameters between different atomic configurations, and so on [16]. A very important point is that, for disordered systems described by TB Hamiltonians, the real-space methods, like the recursion method (RM) of Haydock and co-workers, become robust, with a workload proportional to the size of the system [17] instead of a cubic proportionality, as in the usual band-structure methods, thus providing an effective scheme for the calculations of the electronic structure of amorphous solids with controlled accuracy.

The main step towards constructing the *ab initio* TB Hamiltonian starting from the extended basis set has been made by Andersen and Jepsen [18] on the basis of the well known linear muffin-tin orbital (LMTO) method [19]. The LMTO χ_{RL} (where the subscripts R and L denote the site and the angular-momentum character of the orbital, respectively) are the solutions of the Laplace equation beyond the muffin-tin (MT) spheres at sites R,

which have long-range tails. Consequently the overlap and Hamiltonian matrices

$$O_{R'L'RL} = \langle \chi_{R'L'} | \chi_{RL} \rangle$$

$$H_{R'L'RL} = \langle \chi_{R'L'} | -\nabla^2 - V(r) | \chi_{RL} \rangle$$

which are long ranged are determined by the so-called structure constants $S^0_{R'L'RL}$. Using the simple analytic properties of the structure constants, it is possible to 'screen' $S^0_{R'L'RL}$ by a simple unitary transformation, i.e. to change the power-law decay with distance to a more rapid exponential decay [18]. The transformation is defined by the chosen parameter set, which allows one to construct both the most localized MTO and the nearly orthonormal (NO) representation. Given the MTO in one representation the MTO in the other representation can be obtained by simple matrix operations [19, 20]. The NO representation is required for use with the recursion method where the normalized basis set is required [17]. Then the calculations of the electronic structure can be carried out self-consistently, in complete analogy with the standard LMTO band structure method [19, 20].

The other central issue is the construction of realistic structural models. In principle, the structure can be varied in parallel with the calculations of electronic structure, reformulated in terms of the classical Lagrangian dynamics of Car and Parrinello [21]. This method was extensively used in *ab initio* molecular dynamics simulations of liquid and amorphous Si [22] and other sp-bonded systems, but the underlying pseudopotential method makes its application to systems with transition metals (TM) impractical. It is worth mentioning that the method was applied recently to studies of liquid copper [23], which required the use of the ultra-soft pseudopotential proposed by Vanderbilt [24]. The special procedure for sampling the rapidly changing functions in the core region allowed them to make use of a cutoff energy comparable with that used in the LAPW method.

Very accurate atomic models of some transition-metal–metalloid (TMM) glassy metals can be constructed with the use of model interatomic potentials and various random packing procedures [25]. They are capable of reproducing all the main features of the radial distribution functions of the TMM (TM = Fe, Co, Ni and M = B, P) [12, 13, 26] and Zr–Be glasses [14] in a wide concentration range and in good agreement with high-resolution neutron diffraction data.

The real-space TB-LMTO method (RS-TB-LMTO) was first applied in its simplest form (with 'screened' structure constants interpolated from the crystal data) to some metallic glasses by Fujiwara [27], and then to some amorphous systems, including a-Si [28]. A detailed account of the method and effects of various approximations was given recently by Nowak and co-workers [29], with a thorough investigation of the paramagnetic electronic structure of amorphous $Fe_{80}B_{20}$. We present below a concise description of the method as it has been used in the present work for spin-polarized calculations (section 2), and then proceed to a discussion of results in section 3. The RS TB-LMTO method turns out to be very accurate in describing the electronic states of amorphous solids and their trends with composition. We present the results of paramagnetic and ferromagnetic electronic structure calculations for $Fe_{80}B_{20}$ (section 3.1), $Ni_{100-x}B_x$ (section 3.2) and Zr_xBe_{100-x} (section 3.3). As the comparison with available photoemission data will show, the results for the Fe–B glass are much more reliable than those obtained within the semi-empirical Hubbard model. Section 3 concludes with a comparison between the calculated electron densities of states at the Fermi level and the low-temperature experimental data (section 3.4). A summary of the results is presented in section 4.

2. Electronic structure calculations with the tight-binding LMTO

The standard LMTO basis is *minimal*, i.e. it consists of only nine orbitals for the spd elements and it is *complete* for the atomic sphere for which it is constructed [19]. It is achieved by a smooth matching of the *envelope* functions to the linear combination of $\phi_\nu(r)$ and $\dot{\phi}_\nu(r)$, which are the radial solution and its first energy derivative, respectively, of the Schrödinger equation for an arbitrarily chosen energy E_ν. Thus constructed, the LMTO χ_{RL} is exact in linear order of the energy deviation $(E - E_\nu)$ and is quite accurate in a region about 1 Ryd wide (given by the value of the potential parameter $p^{-1/2}$, see tables 1 and 2). The tail of the LMTO χ_{RL} in the interstitial region is the solution of the Schrödinger equation for a flat potential, i.e. of the Hankel equation $(-\nabla^2 + \kappa^2)\chi_{RL} = 0$, where κ^2 is the kinetic energy of an electron. A reasonable approximation is to use the geometry of atomic spheres (ASA) and take $\kappa^2 = 0$. Then the envelope function K^0 and the second fundamental solution, J^0, become (using the notation of [20, 30])

$$K_L^0(r_R) = \left(\frac{r_R}{w}\right)^{-l-1} Y_L(r_R) \qquad J_L^0(r_R) = \frac{1}{2(2l+1)}\left(\frac{r_R}{w}\right)^{l} Y_L(r_R) \tag{1}$$

where $r_R = |r - R|$, R is the centre of the MT sphere where the envelope functions are defined, w is the mean Wigner–Seitz radius of a system, and Y_L is the usual spherical harmonic. The rule for expansion of the envelope function near the MT spheres, centred at $R \neq R'$, is given by the so-called LMTO structure constants S^0, which decay with distance as $|R' - R|^{-l'-l-1}$ and are obviously long range. We can, nevertheless, perform a linear mixing of the initial fundamental solutions, K^0 and J^0, to suppress the long-range tails of K^0 and make the structure constants (and, consequently, the Hamiltonian and overlap matrices) short range [18]. This procedure can be seen as a unitary transformation of the initial basis set if

$$S^\alpha = S^0 + S^0\alpha S^\alpha = \frac{1}{\alpha}\left(\frac{1}{\alpha} - S^0\right)^{-1}\frac{1}{\alpha} - \frac{1}{\alpha}. \tag{2}$$

In our calculations we have used the spd set of screening parameters [18, 20] ($\alpha_s = 0.348\,50$, $\alpha_p = 0.053\,03$, $\alpha_d = 0.010\,71$, $\alpha_{l>2} = 0$) and the sp set ($\alpha_s = 0.287\,23$, $\alpha_p = 0.025\,82$, $\alpha_{l>1} = 0$) to produce site-*independent* and site-*dependent* types of screening, as described below.

Table 1. Self-consistent potential parameters for $Fe_{80}B_{20}$ and $Zr_{60}Be_{40}$, and the number of states at the Fermi level, n_F.

Rydberg	$c - E_\nu$	d	o^{-1}	$p^{-1/2}$	n_F
Fe s	0.207	0.146	−1.62	5.1	0.63
Fe p	0.597	0.064	−1.39	6.5	0.92
Fe d	0.058	0.019	1.59	0.8	6.58
B s	−0.072	0.210	4.61	6.3	0.88
B p	0.687	0.098	4.55	5.2	1.59
Zr s	0.161	0.084	−0.76	3.6	0.64
Zr p	0.341	0.033	−0.62	4.1	0.72
Zr d	0.228	0.029	−1.01	1.2	2.61
Be s	0.153	0.145	−5.26	4.8	0.77
Be p	0.605	0.040	−3.13	4.3	1.27

Table 2. Self-consistent potential parameters for $Ni_{100-x}B_x$ and the number of states at the Fermi level, n_F. The results of spin-polarized calculations for different spin projections are denoted by arrows.

$100-x:x$		$c-E_\nu$	d	o^{-1}	$p^{-1/2}$	n_F
a-Ni	Ni $s_\uparrow$	0.190	0.152	−2.11	4.9	0.29
	Ni $s_\downarrow$	0.187	0.153	−2.12	4.9	0.30
	Ni $p_\uparrow$	0.665	0.064	−1.72	6.6	0.28
	Ni $p_\downarrow$	0.664	0.065	−1.74	6.6	0.30
	Ni $d_\uparrow$	0.013	0.009	0.70	0.6	4.64
	Ni $d_\downarrow$	0.027	0.010	0.75	0.6	4.19
80:20	Ni s	0.212	0.162	−2.05	5.4	0.58
	Ni p	0.686	0.071	−1.74	7.0	0.71
	Ni d	0.029	0.014	1.11	0.8	8.51
	B s	0.141	0.138	−1.68	3.9	1.16
	B p	0.532	0.033	−1.17	4.3	2.65
75:25	Ni s	0.215	0.166	−2.04	5.5	0.56
	Ni p	0.689	0.073	−1.75	7.1	0.66
	Ni d	0.029	0.015	1.16	0.8	8.54
	B s	0.160	0.137	−1.64	4.0	1.13
	B p	0.536	0.032	−1.14	4.4	2.60
66:34	Ni s	0.237	0.171	−2.03	5.8	0.55
	Ni p	0.712	0.074	−1.73	7.5	0.68
	Ni d	0.030	0.017	1.28	0.8	8.54
	B s	0.126	0.151	−1.72	4.1	1.09
	B p	0.529	0.041	−1.27	4.4	2.35

Matching the envelope functions (1) at all the atomic spheres to $\phi_{\nu RL}$ and $\dot{\phi}_{\nu RL}$ we arrive at the following working expression for the LMTO:

$$\chi^\alpha_{RL} = \phi_{\nu RL} + \sum_{R'L'} \dot{\phi}^\alpha_{\nu R'L'} h^\alpha_{R'L'RL} + \kappa_{RL} \tag{3}$$

where κ_{RL} is the interstitial part of the LMTO, and

$$\dot{\phi}^\alpha_\nu = \dot{\phi}_\nu + \phi_\nu o^\alpha \tag{4}$$

where the important potential parameter o^α shows to what extent the new 'screened' representation is orthogonal to the standard one, $o^\alpha = \langle \phi_\nu | \dot{\phi}^\alpha_\nu \rangle$, where brackets stand for the integration over the given MT sphere (here and below we omit the orbital index l for the sake of convenience).

The *two-centre* Hamiltonian h^α plays a central role in the TB-LMTO method because the usual overlap and Hamiltonian matrices are expressed through it, as are the matrices of potential parameters (diagonal in RL space) [20]. The explicit expression is given by

$$h^\alpha = c^\alpha - E_\nu + \sqrt{d^\alpha} S^\alpha \sqrt{d^\alpha}. \tag{5}$$

One can always determine a set of α for which the LMTOs become *nearly orthonormal*, i.e. where $\alpha = \gamma$ and $o^\gamma = 0$. This representation (we will denote it by the superscript γ) is not universal and depends on the values and slopes of ϕ_ν and $\dot{\phi}_\nu$ on the MT sphere, which also define the rest of the potential parameters c^α, d^α and o^α [20]. Hence the construction of the NO representation can be done most conveniently by starting from the 'most localized'

TB Hamiltonian, which is particularly short ranged, and then transforming it to the NO γ-representation [20, 30]. The total Hamiltonian in the NO representation has the form

$$H^{\gamma} = E_{\nu} + h^{\gamma} = E_{\nu} + h^{\alpha} - h^{\alpha} o^{\alpha} h^{\alpha} + \cdots. \tag{6}$$

This ASA form of the orthonormalized Hamiltonian was used in the present work, with the expansion truncated after the third term to compute the electron density of states in combination with the recursion method. The third *hoh* term in (6) gives a Hamiltonian that is exact to *second order* in $(E - E_{\nu})$. This term may be necessary in systems with wide bands [30], especially for sp states. Although it increases the number of hops from the central atom, we have actually retained only the hops over the neighbours within one screening length with no loss of accuracy. The non-ASA terms omitted in (6) can be calculated for the arbitrary structure in real space [30, 31]. The Hamiltonian (6) is diagonal in spins, and we have therefore suppressed the spin indices in (3)–(6).

Within the local spin-density and atomic-spheres approximations one usually achieves self-consistency for only the spherically symmetric part of the electron density, $n_{R\sigma}(r)$, within the sphere at side R for given spin index σ. The electron density within the MT spheres, $n_R(r)$, is a sum of the density of valence electrons, $n_R^{\mathrm{val}}(r)$, and core electrons, $n_R^{\mathrm{c}}(r)$. The density of valence electrons can be easily found from the first moments of the local electron DOS and the MTOs within the given sphere [19]. Thus the following expression holds for the sum of the Hartree and exchange-correlation potentials inside the sphere at site R:

$$V_{R\sigma}(r) = -\frac{2Z_R}{r} + \int_{s_R} \frac{2n_R(r')}{|r - r'|} \mathrm{d}^3 r' + \mu_{\mathrm{xc},\sigma}[n_{R\uparrow}(r), n_{R\downarrow}(r)] - \sum_{R \neq R'} \frac{2z_{R'}}{|R - R'|}. \tag{7}$$

Here Z_R is the nuclear charge, and z_R is equal to the nuclear charge Z_R minus the number of electrons in the sphere. There is some complication concerning the evaluation of the Madelung potential (the last term in (7)), which at site R is

$$-\sum_{R \neq R'} 2z_{R'}/|R - R'|. \tag{8}$$

The Ewald summation method can be extended for the evaluation of this Madelung contribution for a topologically disordered structure, but it requires the radial distribution functions and the structure factors for the given structure [32] as well, and this makes the method impractical. It was suggested earlier by Nowak and co-workers [29] that the same averaged Madelung potential should be used for all atoms of the same type, this being approximated by integrating the radial distribution functions. In the present work and in our code we applied a different strategy in order to keep all the information about the local atomic coordination. To this end, we have performed a *direct summation* in (8) over the neighbours included in the definition of the Hamiltonian (6) and *integrated* over the rest of the system with calculated radial distribution functions. For an atom of type i at the origin the latter is

$$-2 \int_{R_c} \left[z_i n_i g_{ii}(R') + z_j n_j g_{ij}(R') \right] 4\pi R' \mathrm{d}R' \tag{9}$$

where the g_{ij} stand for the radial distribution functions, n_i is the number density of atoms of type i and R_c is our cutoff radius. We believe that the two-step evaluation of the Madelung

term is more precise than performing only the integration over radial distribution functions (9), as suggested in [29].

Given the initial charge densities, we have concurrently calculated the projected density of states for both spin directions:

$$n_{Rl\sigma}(E) = -\frac{1}{\pi}\mathrm{Im}\left(\frac{1}{E + \mathrm{i}0 - \hat{H}^{\gamma}}\right)_{Rl\sigma,Rl\sigma} \tag{10}$$

where the Hamiltonian operator $\hat{H}^{\gamma}$ is described in (6). The DOS was computed using the recursion method [17], which approximates the imaginary part of the Green function (10) by a continued fraction. We have used the linear predictor scheme of Allan [33] to terminate the continued fraction generated by the procedures for the estimation of the band edges after Nex [34] and Beer and Pettifor [35]. The new potential calculated from (7) with the use of the charge densities for both spin directions is then mixed with an old one for the next iteration until self-consistency is achieved. The present scheme is a generalization of the recently reported method of paramagnetic calculations by Nowak and co-workers [29] for the case of spin-polarized calculations, which we implemented in our code. Other details of the present calculations are described below.

3. Results and discussion

For calculations of the electronic structure with the RS-TB-LMTO method we have used structural models constructed by means of the Monte Carlo simulation of quenching from the melt and relaxation at constant temperature, as described elsewhere [12–14]. We have used simple pairwise model interatomic Morse-type potentials [26], which we found to be very accurate in reproducing the high-resolution experimental data for the radial distribution functions (RDF). For Ni–B and Zr–Be glasses the parameters of the potential are given in [12–14]. The extensive full-potential LMTO calculations have shown that the electron density inhomogeneity due to the strongly covalent TM d–B p bonds produces a moderate effect on the electron density of states and that the DOS shape near the Fermi level [36] remains practically unaffected in comparison with the ASA-LMTO calculations. This provides a justification for the use of the ASA-TB-LMTO method for studying the density of states in amorphous borides.

In our present electronic structure calculations we have followed the scheme described in section 2 for constructing the basis set and the self-consistent electron density and potential parameters for atoms of a given sort. For the self-consistent calculations of the electron potential we have used the moments of the DOS averaged over about ten atoms of the given element, taken close to the centre of a cluster. We have also taken up to 50 atoms for averaging and showed that ten atoms is already enough to get convergent results. It was shown in recent studies of 40-atom amorphous Zr clusters [37] that, at least in monatomic systems, the total DOS is rather insensitive to this averaging procedure, with enhanced screening of the local atomic charges.

The 'screened' structure constants S^{α} were found from (2) by a direct inversion of the subclusters containing 20–25 nearby atoms around each site in a simulated cell of 500 atoms with periodic boundary conditions (Nowak and co-workers have considered somewhat smaller 16-atom subclusters in the 400-atom calculated cell). It is worth mentioning that an approximate way of calculating S^{α} leads to an overestimate of the height of the DOS peaks as in [27] (see the detailed analysis in [29]). The DOS was calculated with the Hamiltonian (6) with the inclusion of the *hoh* term. It was then used to produce the sequence of L_s, L_p and L_d pairs of continued fraction coefficients (CFC) for s, p and d states, respectively.

3.1. $Fe_{80}B_{20}$: paramagnetic and ferromagnetic LDA calculations

We first discuss the results of our paramagnetic calculations for a-$Fe_{80}B_{20}$ glass where a detailed comparison with previous calculations is available [29] to check the present calculational scheme. The picture of the paramagnetic density of states (figure 1) is in overall agreement with the previous results [29] if we make use of the site-*independent* spd screening constants to calculate S^{α} and retain spd MTOs for Fe and sp MTOs for B in our 500-atom model. The remaining minor differences can presumably be attributed to features of the structural models used and reflect the procedure of obtaining the amorphous state. To obtain our structural model we have simulated directly a rapid quench from the melt, whereas Nowak and co-workers [29] made use of the 400-atom model obtained by relaxation of a dense random-packed model with the same interatomic potential.

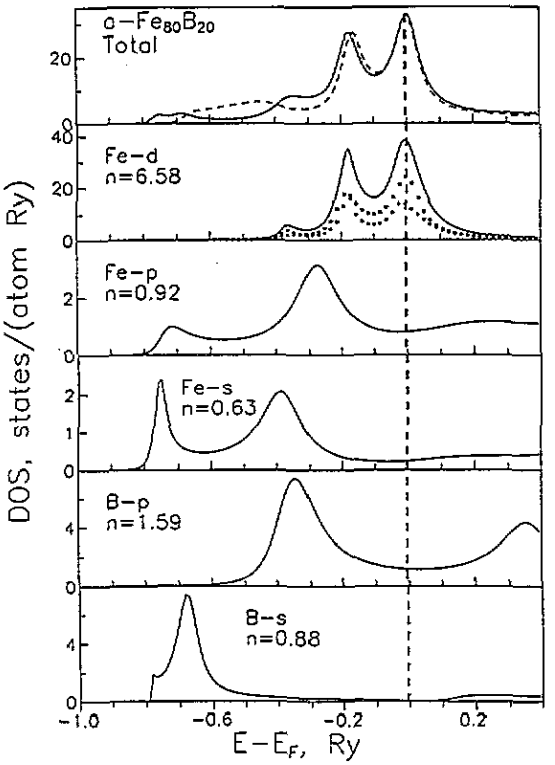

Figure 1. Total and partial electronic densities of states in amorphous $Fe_{80}B_{20}$, calculated with $L_s = L_p = 10$ and $L_d = 18$ pairs of continued fraction coefficients and with site-*independent* spd screening (full curve) and with site-*dependent* screening (broken curve). The partial contributions from $d(e_g)$ and $d(t_{2g})$ states are indicated on the Fe d partial DOS. The ASA radii are $S_{Fe} = 2.703$ au, $S_B = 1.907$ au.

The two-peak DOS shape in the paramagnetic a-$Fe_{80}B_{20}$ corresponds to a non-bonding d band and divides the whole spectrum into lower bonding and upper non-bonding states. The peak in the B p DOS comes from a strong Fe d–B p hybridization that gives rise to a −0.35 Ryd peak and a high occupancy of B p states with $n_{Bp} = 1.59$ (1.41 in [29]). The B s band is split into bonding and antibonding parts with the lowest B s peak at −0.7 Ryd in our model, i.e. at a slightly higher energy than obtained before (−0.8 Ryd [29]). The self-consistent potential parameters and the partial occupation numbers are summarized in table 1. Charge transfer between Fe and B atoms in our calculations is rather small, and can be estimated as $z_{Fe} = -0.13$ and $z_B = +0.52$ (−0.25 and +1.0 in [29], respectively). It is worth mentioning that this charge transfer is not a genuine characteristic of the bonding. We can recall the early picture of the magnetic behaviour of crystalline borides, which was

explained as a result of electron transfer from metalloid to transition metal to gradually fill the TM d band [38]. Similar arguments were evoked to explain the observed trends in the iron-based magnetic glasses [1, 2]. Later, the x-ray experiments on FeB and Fe_2B crystals provided evidence that this simplified picture does not hold, and the bonding has a prominent *covalent* rather than ionic nature [39]. The correspondent covalent TM d–B p interaction is relevant for the observed moment distribution over the unit cell [39]. The competition between metallic d–d bonds between transition metals and covalent d–p bonds between transition metal and metalloid explains the composition dependence of the moment on the TM site [36, 40].

Present calculations give almost the same results for paramagnetic DOS in $Fe_{80}B_{20}$, as obtained recently by Nowak and co-workers [29]. We clearly see that boron s and p bands are split into lower bonding and upper bonding parts, and that there is no donation of the B p electron to Fe as expected in a picture of ionic bonding.

The double-peak DOS shape of the amorphous $Fe_{80}B_{20}$ is typical of the glassy TM–B systems; therefore, it is worth investigating its physical nature. It is interesting to mention that the use of site-*dependent* screening in (2) (spd for Fe sites and sp for B sites) results only in moderate changes of the DOS far below the Fermi level (figure 1). Nowak and co-workers [29] found no correlation between the Fe d double hump and the local radial distribution function. Recalling the simple multiple-scattering picture of the formation of electronic states in solids, one could have expected the involvement not only of the radial correlations but also of the bond-angle distribution in the formation of the DOS shape. In our previous studies we have shown, by analysing Steinhardt's bond-angle parameters, that the local cubic coordination is almost lost in the amorphous state, which is closer to liquid structure [12]. To look for some traces of the former crystalline order we have inspected the population of lower and upper Fe d peaks by states of e_g and t_{2g} symmetry. It is well known that they are responsible for higher- and lower-energy peaks in the BCC Fe d DOS, respectively (see, for example, figure 1 in [27]). It is very interesting that, in the amorphous phase, this asymmetry in the density of e_g and t_{2g} states persists, although their contributions to both humps are now much more symmetrical (figure 1). The e_g states contribute about 60% of the high-energy peak of the d DOS. This asymmetry is very small in comparison with the situation in BCC Fe [27], but it still exists.

The main peak of Fe d states (and a total DOS) in our paramagnetic calculations coincides with the Fermi level (figure 1). The value of our DOS at the Fermi level, $N(0)$, is 32.4 states per atom Ryd, which is bigger than the previous theoretical value of 26 states per atom Ryd [29]. Although the simple Stoner criterion does not indicate the presence of weak ferromagnetism in the system, this DOS shape explains the observed magnetic moment with the use of the generalized Stoner model [29]. In this model we can estimate the moment on the Fe atoms from the following condition, valid for elemental ferromagnets [41]:

$$I\bar{N}(m) = 1. \tag{11}$$

Here $\bar{N}(m)$ is the DOS averaged over the energy interval around the Fermi level that gives the moment m. In an actual procedure one defines the Fermi levels $E_F^{\uparrow}(m)$ and $E_F^{\downarrow}(m)$ in order to satisfy the conditions

$$\tfrac{1}{2}m = \int_{E_F^{\downarrow}}^{0} N(E)\,\mathrm{d}E = \int_{0}^{E_F^{\uparrow}} N(E)\,\mathrm{d}E \tag{12}$$

where E is the energy with respect to the Fermi level. Then

$$\bar{N}(m) = m/(E_F^{\uparrow} - E_F^{\downarrow}) \tag{13}$$

and (11)–(13) represent a self-consistent set of conditions giving the value of the magnetization.

We first analysed the possible ferromagnetic behaviour of compounds studied by making use of the generalized Stoner model and accounting only for the transition-metal states, since other contributions around the Fermi level are negligible. Accordingly, all the quantities involved in (11)–(13) should be regarded as site- and orbital-dependent quantities for the given kind of atom. A simple analysis shows that the solution of (11) exists only in the case that $N(E)$ changes sharply around the Fermi level and has a substantial magnitude. It cannot be satisfied with a flat DOS near E_F. The most important feature of the generalized Stoner model is that it is capable of revealing the actual ferromagnetic behaviour, even in cases where the standard Stoner condition fails, as is the case in amorphous $Fe_{80}B_{20}$. The disadvantage of the model is the sensitivity of the moment to the actual value of the Stoner parameter I, which is not precisely known. We have applied the generalized Stoner model to the iron–boron and nickel–boron systems, with $I = 65$ mRyd for Fe and $I = 72$ mRyd for Ni [41]. For the net magnetic moment on the Fe site in $Fe_{80}B_{20}$ we obtained the value $\bar{\mu} = 2.05\mu_B$/Fe, which is slightly smaller than the value $\bar{\mu} = 2.20\mu_B$/Fe estimated by Nowak and co-workers [29], where the latter is almost equal to the moment in BCC Fe.

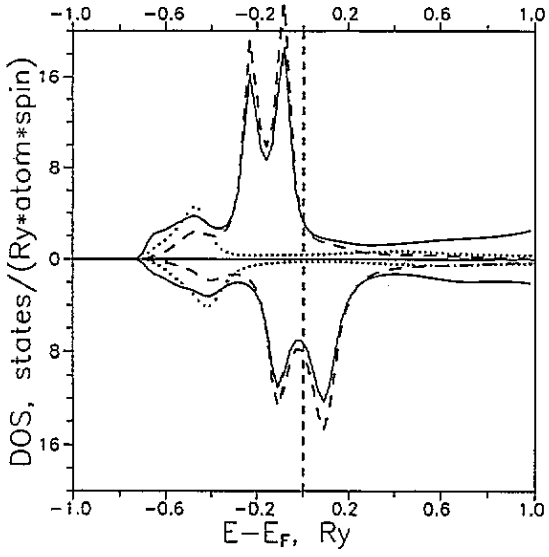

Figure 2. Spin-polarized electronic densities of states in amorphous $Fe_{80}B_{20}$: total DOS (full curve), Fe d DOS (broken curve) and B p DOS (dotted curve). The parameters are the same as in figure 1.

Second, we have performed the *direct* LSD spin-polarized calculations, which we did with our spin-polarized code with results presented in figure 2. We see that the DOS in $Fe_{80}B_{20}$ is subject to strong ferromagnetic splitting, producing a net moment $\bar{\mu} = 2.14\mu_B$/Fe that is slightly bigger than our Stoner estimate ($2.05\mu_B$/Fe) and somewhat less than the saturated value of the moment in BCC Fe ($2.214\mu_B$). There is substantial scatter in experimental data on the net moment of Fe: $\bar{\mu}$=2.0 [2], 2.15 [42], 1.97 [43], 1.80 [44] and 2.23 μ_B [45]. The averaged experimental value is 2.03 μ_B/Fe, which is very close to our calculated LSD value $2.14\mu_B$/Fe. Boron sp bands are slightly negatively polarized, with the net moment of the boron sites being $-0.06\mu_B$.

We are now in a position to perform a detailed comparison with high-precision photoemission data [7]. Our ferromagnetic DOS has a strong peak at −1 eV with a left satellite peak at −3 eV. The B sp together with Fe s states produce a shoulder at 5.5–6.5 eV

below the Fermi level. It should be noted that Nowak and co-workers [29] predicted the shoulder at −3 eV, whereas we have a pronounced peak there. Above the Fermi energy we have the empty minority spin band peak, which lies at +1 eV. We are not aware of experimental observations of that peak, which should be observable by inverse photoemission. It is worth mentioning that the Hubbard-model calculation [46] gives a one-peak DOS shape for $Fe_{80}B_{20}$ and it is, therefore, in contradiction with the photoemission and other data.

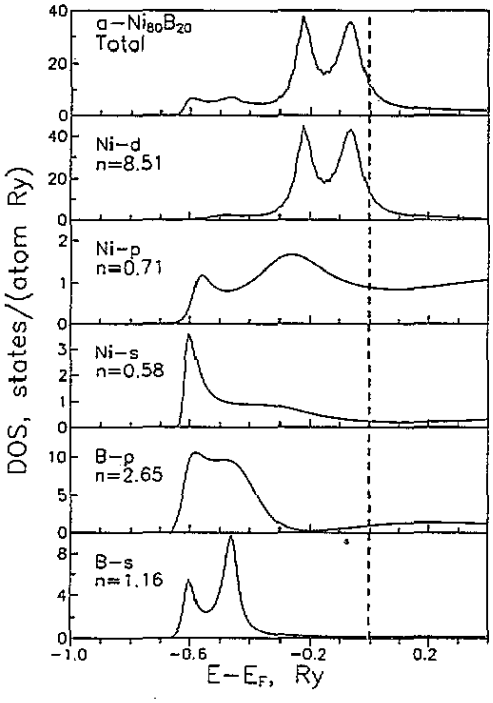

Figure 3. Total and partial electronic densities of states in amorphous $Ni_{80}B_{20}$, calculated with $L_s = L_p = 10$ and $L_d = 18$ pairs of continued fraction coefficients and with site-*dependent* screening. The ASA radii are $S_{Ni} = 2.551$ au, $S_B = 2.316$ au.

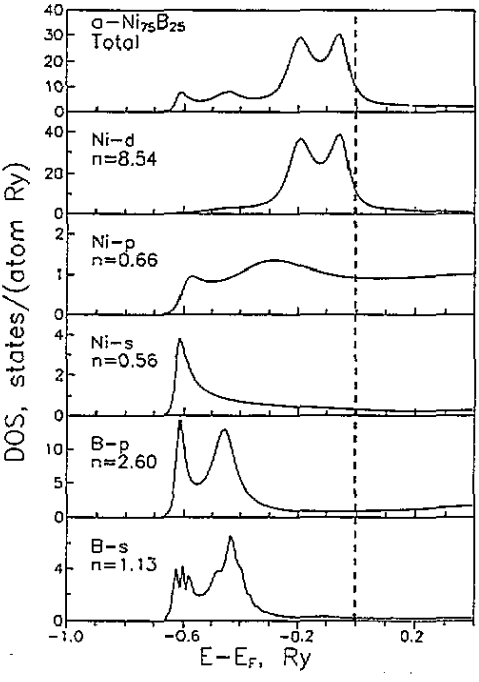

Figure 4. Total and partial electronic densities of states in amorphous $Ni_{75}B_{25}$: total DOS (full curve) and Ni d DOS. The ASA radii are $S_{Ni} = 2.534$ au, $S_B = 2.300$ au.

3.2. $Ni_{100-x}B_x$: weak ferromagnetism

The results of our calculations for a-$Ni_{100-x}B_x$ are summarized in figures 3–6 and table 2. As one would have expected, the electronic structure of amorphous $Ni_{80}B_{20}$ resembles that of $Fe_{80}B_{20}$ apart from a rigid shift of the DOS downwards with respect to the Fermi level E_F, as a result of substitution of Fe by Ni with two extra d electrons. The high-energy peak is now at −0.07 Ryd and the DOS value at the Fermi level, $N(0)$, is low and incompatible with the existence of a moment of the Ni atoms (figure 3). With increasing dilution by boron atoms the main change in the DOS is a gradual decrease of the weight of the double peak formed by Ni d electrons and an increase of the B partial DOS (figures 3–6). The B p DOS has a rectangular form with two low-energy peaks of the total DOS, at −0.45 and −0.6 Ryd in a-$Ni_{80}B_{20}$ (figure 3). The height and weight of the B p DOS gradually grows

at the expense of the Ni d-states and broadens by 0.2 Ryd in a-$Ni_{66}B_{34}$ (figure 5). One can correlate this broadening with a *decreasing* mean distance between neighbouring boron atoms. In the present calculations the boron sites acquire some negative charge, which *decreases* with an increase of the boron content from −0.81 in a-$Ni_{80}B_{20}$ down to −0.44 in a-$Ni_{66}B_{34}$.

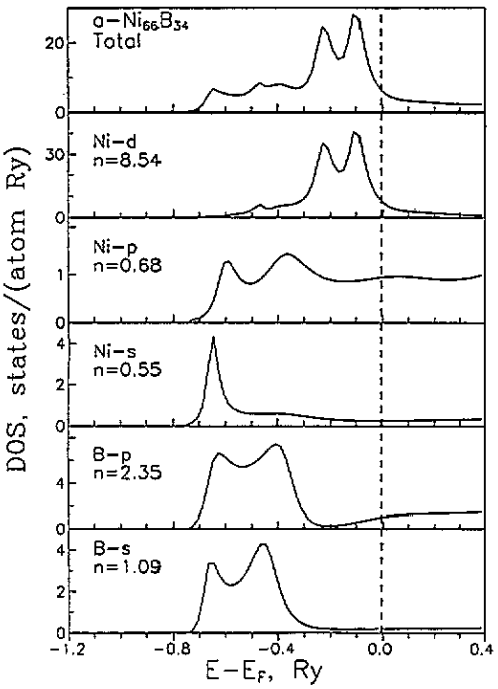

Figure 5. Total and partial electronic densities of states in amorphous $Ni_{66}B_{34}$. The ASA radii are S_{Ni} = 2.493 au, S_B = 2.264 au.

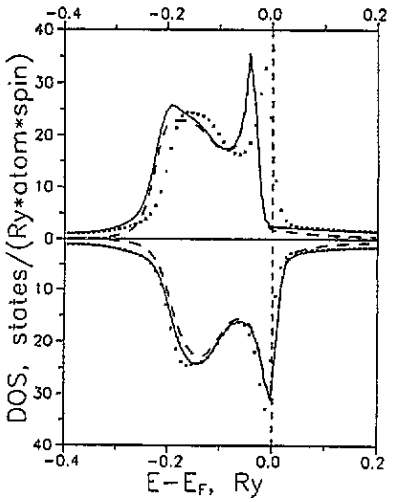

Figure 6. Total and partial spin-polarized electronic densities of states in amorphous pure Ni: total DOS (full curve) and d states (broken curve). The paramagnetic DOS is given for comparison (crosses).

It turns out that the electronic structure of amorphous $Ni_{66}B_{34}$ is analogous to that of its crystalline counterpart c-Ni_2B, in spite of significant changes in the local order in the Ni_2B system under amorphization [12, 13]. It is worth mentioning that the electronic structure of c-Ni_2B is very similar to the electronic structure of Fe_2B [36, 39, 40]. In c-Ni_2B local order consists of eight Ni atoms forming an Archimedian antiprism around each B atom. There are no B–B pairs in the crystal, but they evolve under amorphization (the experimental value of the B–B coordination number varies between $Z_{BB} = 0.9 \pm 0.1$ [10] and 1.1 [11]). Our simple model is capable of reproducing the main features of the RDFs in amorphous Ni_2B [12–14]. In contrast to the local order of the 'classical' $TM_{80}M_{20}$ composition, where the atoms of the metalloid occupy the 'hollows' left by the big metal atoms and direct contact of metalloid atoms does not exist, in a-TM_2M M–M contact does exist and it signals a sort of 'frustration' of packing of the small atoms. The RDFs of the boron atom in $Ni_{66}B_{34}$ show direct B–B contact, with the first maximum at 1.7 Å and a corresponding coordination number $Z_{BB} = 0.75$. This peculiar structure presumably arises from the interference in the packing of unlike atoms in the range 2–2.5 Å. Taking into account this behaviour we would

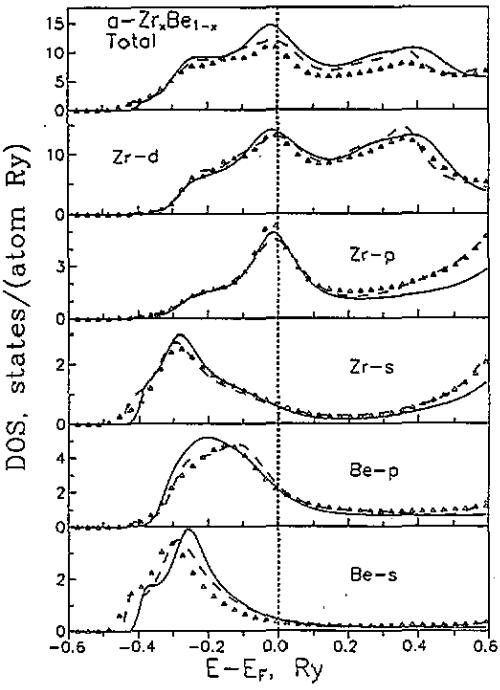

Figure 7. Total and partial electronic densities of states in amorphous Zr_xBe_{100-x}, calculated with $L_s = L_p = 10$ and $L_d = 18$ pairs of continued fraction coefficients and with site-*dependent* screening: $x = 70$ (full curve), $x = 60$ (broken curve), $x = 50$ (triangles). $S_{Zr} = 3.491$ au, $S_{Be} = 2.363$ au.

have expected some changes in the role of the B 2p–Ni 3d hybridization compared with that for the $TM_{80}M_{20}$ composition.

The DOS in the crystalline counterpart, Ni_2B, studied by the full-potential LMTO method, consists mainly of two peaks, at about −0.1 Ryd and −0.25 Ryd, respectively [36]. The DOS washes out under amorphization but still preserves the double-peak structure mainly formed by d electrons, as in $Fe_{80}B_{20}$ discussed above. The B s and p partial DOS show the broad double-peak structures in the interval from −0.7 to −0.4 Ryd formed by covalent bonding with Ni sp bands (figures 3–5). By analogy with the $Fe_{80}B_{20}$ glass one can see that the interaction between metal and metalloid atoms has a strongly covalent character that splits B sp states into lower bonding and upper antibonding pairs, and so no donation of electrons from B to Ni actually exists. Inspection of figures 3–5 shows that the main B p DOS peak in the energy interval from −0.6 to −0.4 Ryd is actually affected by the changes in atomic structure under amorphization. The covalent p–d bonding becomes more pronounced, the height and width of the B p DOS peak grows, but the metallic bonding between transition metal atoms still dominates. Recently, we have calculated the x-ray absorption fine structure (XAFS) spectra for a-$Ni_{66}B_{34}$ with the use of the self-consistent potentials in comparison with c-Ni_2B, and showed the large effect of amorphization on the low-energy (multiple-scattering) part of the XAFS. This effect is particularly high for the B K edge since the local coordination of boron atoms changes drastically in amorphous phase with respect to the crystal [47].

We can compare the calculated DOS of $Ni_{80}B_{20}$ with photoemission spectra taken from amorphous $Ni_{78}P_{14}B_8$ [8]. As was pointed out by Amamou and co-workers [8] the PES for the amorphous Ni–P–B system is very similar to that of elemental Ni and crystalline Ni_3B and Ni_3P. We can, therefore, expect that our comparison with these data is reasonable. The main experimental peak lies close to E_F (0.7 eV) with a shoulder at 1.6 eV, whereas for the calculated DOS of $Ni_{80}B_{20}$ the main peak is at 0.95 eV and the left peak is at 3.0 eV

(figure 3). We can rather confidently attribute the band broadening and total shift to the LDA shortcomings. That is, comparison of the band calculations with experiment for the elemental Ni shows that LDA leads to a broadening of the d band by 1.1 eV and its shift by 0.25 eV to lower energies (see the recent discussion in [48]). We believe that the same omission of non-locality and dynamical correlations in the LDA method is responsible for the broadening and shift of the Ni d band in $Ni_{80}B_{20}$ glass.

Simple inspection of figures 3–5 for the DOS in Ni–B glasses and application of the Stoner criterion shows that these glasses are paramagnetic, in agreement with experiment [3,4]. At the same time the hypothetical pure a-Ni is ferromagnetic, with a net moment $\bar{\mu} = 0.43\mu_B$ and a small exchange splitting $\bar{\mu}I = 0.4$ eV (figure 6). This value is slightly less than the moment in FCC Ni ($0.6157\mu_B$). The striking fact about the a-Ni DOS is that the main peak of the minority spin band almost coincides with E_F. Usually such a system tends to lower the high band energy by undergoing some structural phase transition to avoid this coincidence. In the case of Ni, however, this tendency is in competition with the ferromagnetic splitting energy, which pushes the minority band towards E_F, resulting in a weak itinerant ferromagnetism in a-Ni. To illustrate the effect of ferromagnetic splitting on the DOS of a-Ni we present in figure 6 both ferromagnetic and paramagnetic solutions. In fact, this ferromagnetism is so weak that it always disappears in the presence of a small amount of paramagnetic alloying element. From the experimental data on Ni–B [3,4] and Ni–P [5] glasses this is known to occur.

The compositional behaviour of the electronic structure of amorphous nickel borides is clearly responsible for the marginal behaviour of the nickel moment: with two extra d electrons compared to iron compounds, the DOS peak is pulled away from the Fermi level and an addition of about x_c=17 at.% of metalloid atoms is enough to kill the net Ni magnetic moment [5]. It should be mentioned that the site-projected DOS is subject to pronounced local variations [29], hence *locally* the $N(0)$ might get enhanced due to short-range order fluctuations and the corresponding areas can show increased Pauli paramagnetism or even acquire local moments. By considering the effects of magnetic precipitates (inhomogeneities), one can probably attribute the local variations in electronic structure to the appearance of giant-moment paramagnetic clusters above some critical concentration x_c of metalloid atoms, and superparamagnetic particles below x_c, as takes place in Ni–P glasses with $x_c = 17$ at.%P [5].

3.3. Zr_xBe_{100-x}

Amorphous Zr_xBe_{100-x} belongs to the separate class of metallic glasses formed by a transition and a simple metal. This system was recently extensively studied experimentally and showed interesting dynamical and electronic properties as a function of composition [14]. As a result of the large size difference between Zr and Be atoms, the Be atoms are always in direct contact even at 30 at.% Be and the DOS shape changes gradually with x. The Be s electrons hybridize with the Zr d electrons and this results in a Be DOS peak at about -0.3 Ryd. The DOS at the Fermi level is dominated by Zr d electrons, which form a rather broad peak at E_F with a left shoulder at -0.25 Ryd that confirms the usual metallic interaction between Zr atoms (figure 5; see figure 7). This result is in agreement with recent calculations of pure a-Zr [37]. It is worth emphasizing that no tendency to form a depleted DOS or to avoid the maximum of the DOS at the Fermi level is seen in Zr–Be glass, where a larger role from sp bonding could have been expected, i.e. the well known arguments of Nagel and Tauc do not apply for the stability of the transition-metal–simple-metal glasses.

3.4. Comparison with low-temperature experiments

Quantitative information on the density of states and its compositional dependence is provided by low-temperature specific heat and magnetic susceptibility measurements. As is well known, at low temperatures the electronic specific heat and paramagnetic susceptibility can be expressed via the density of states at the Fermi level, $N(0)$. Correcting the classical expressions with respect to electron–phonon enhancement, λ, and the Stoner exchange enhancement, I, we can write down the following expressions for the electronic specific heat, C_e, and the Pauli susceptibility, χ_P:

$$C_e = \gamma_e T \qquad \gamma_e = \tfrac{1}{3}\pi^2 k_B^2 N(0) \tag{14}$$

where the electron–phonon coupling λ renormalizes the LDA density of states we have discussed in previous sections:

$$N(0) = (1+\lambda)N_{LDA}(0). \tag{15}$$

The density of states estimated from the Pauli susceptibility subject to Stoner exchange enhancement with the parameter I that we have already used is

$$\chi_P = \mu_B^2 N(0) \qquad N(0) = N_{LDA}(0)/[1 - I\tfrac{1}{2}N_{LDA}(0)]. \tag{16}$$

The enhancement factors can be estimated independently, hence (15) and (16) provide a direct test of the calculated $N(0)$ in comparison with experiment. The coupling constants λ for pure Ni and Zr were estimated from resistivity measurements to be 0.8 and 1.1, respectively [49] and, in this simple approximation, we shall neglect a small contribution from simple-metal/metalloid electrons on the Fermi level and only account for the actual concentration of the transition metal in a given alloy. As for the Stoner parameter, this is an almost atomic quantity and we shall make use of the same values for Ni and Fe as we did before (72 and 65 mRyd, respectively).

Table 3. Theoretical and experimental values of the density of states at the Fermi level, $N(0)$, for Ni–B and Zr–Be glasses.

	$Ni_{80}B_{20}$	$Ni_{75}B_{25}$	$Ni_{66}B_{34}$	$Zr_{70}Be_{30}$	$Zr_{60}Be_{40}$	$Zr_{50}Be_{50}$
$N_{LDA}(0)$	11.5	9.4	5.9	14.2	11.9	10.7
$N(0)$, (15)	18.9	15.0	9.0	25.1	19.8	16.6
Exp., C_e	20.0 [50,51]	16.3 [50,51]	9.3 [50,51]	21.4 [14]	18.04 [14]	14.04 [14]
$N(0)$, (16)	19.6	14.2	7.5	—	—	—
Exp., χ_P	22.4 [3]	18.1 [3]	12.7 [3]	—	—	—

The values, calculated for the bare and enhanced $N(0)$ in Ni–B and Zr–Be are presented in table 3. All estimated $N(0)$ values are in a very good agreement with experiment for all glasses studied when the enhancement factors are taken into account. It is especially interesting because, in the case of the Ni–B system, measurements have been made for both the electronic specific heat [50,51] and the magnetic susceptibility [3,4], thus providing a cross-check of calculated quantities. We can therefore conclude from table 3 that the renormalized LDA values for $N(0)$ are in very good agreement with experiment, provided that the enhancement factors for either electron–phonon interaction or spin fluctuations are

taken into account. It should be noted that theoretical values are systematically below the experimental ones, but the differences are nearly the same as those between the experimental values obtained from different methods. The Zr–Be data from the electronic heat capacity are reproduced equally well. In a-$Fe_{80}B_{20}$ the experimental value amounts to 38.5 states per Ryd atom [52], whereas LDA predicts 32.4 states per Ryd atom for paramagnetic $Fe_{80}B_{20}$ and 11.1 states per Ryd atom for the spin-polarized phase. This discrepancy cannot be completely explained by an electron–phonon enhancement factor and, therefore, it might indicate a significant effect of spin fluctuations in Fe–B systems. Concluding, we see that the overall agreement between the calculated and experimental DOS in Ni–B and Zr–Be glasses demonstrates the accuracy of the present method in describing the electronic properties of disordered metallic systems.

4. Conclusion

We have presented self-consistent real-space TB-LMTO calculations for the amorphous systems $Fe_{80}B_{20}$, $Ni_{100-x}B_x$ and Zr_xBe_{100-x}. The density of states near the Fermi level is dominated by the d electrons of the transition metal in all these glasses. These states near E_F are formed by non-bonding d orbitals, which divide the whole electron spectrum into the bonding (below) and anti-bonding (above) states. Strong covalent interaction between the TM d and the metalloid/simple atom p electrons then defines the shape of the low-energy part of the density of states. The DOS is somewhat smeared out with respect to the crystalline counterpart and deformed in accordance with the changes in local order under amorphization. This is the case even in systems with a large content of metalloid, like Ni_2B, where direct B–B contact evolves under amorphization, which is virtually non-existent in $TM_{80}M_{20}$ glasses. The corresponding increase in the importance of covalent p–d bonding between B and Ni was traced in a series of a-$Ni_{100-x}B_x$ glasses, where the weight and width of the B p band gradually increases with x. In Ni- and Fe-based borides the DOS has a similar two-peak form near the Fermi level. This behaviour seems to be generic to the transition-metal–metalloid glasses, and it is analogous to that of crystalline TMM compounds, where some competition between TM d–TM d and TM d–M p interactions takes place [53].

The above-mentioned features of the electron density of states provide a simple insight into the quite different magnetic behaviour of Fe- and Ni-based glasses. The main high-energy peak of the $Fe_{80}B_{20}$ *paramagnetic* DOS is very close to the Fermi level, which results in a high net magnetic moment on the Fe site, as already predicted from the generalized Stoner model [29]. The estimate of the Fe net moment within the Stoner model gives $\bar{\mu} = 2.05\mu_B$/Fe (2.20 μ_B/Fe in [29]). We have also calculated the Fe moment within the local spin-density approximation and the result $\bar{\mu} = 2.14\mu_B$/Fe is in very good agreement with experiment. Thus, the amorphous iron borides are strong itinerant ferromagnets just like their crystalline counterparts [36,40], with similar trends in magnetic behaviour with composition [54].

The DOS in $Ni_{100-x}B_x$ glasses has a similar two-peak structure, shifted downwards with respect to the Fermi level, which does not allow a magnetic moment to appear on Ni atoms in glasses with x above some threshold x_c. Nevertheless, local concentration and density fluctuations would allow the Ni atoms to form clusters with highly enhanced paramagnetism slightly above x_c in accordance with recent extensive experiments on Ni–P glasses [5]. The calculated pure a-Ni carries a small net moment $\bar{\mu} = 0.43\mu_B$, which disappears upon alloying with metalloids.

Comparison with available PES data on the Ni–B glasses allows us to illustrate the effect of the local density approximation on the electronic structure: the calculated d band

in the Ni–B glass is shifted downwards by 0.25 eV and broadened by 1.1 eV: the situation is equivalent to that in FCC Ni [48].

The Zr–Be metallic glasses fall into the separate class of transition-metal–simple-metal amorphous systems. Here too the (broad) main peak in the electron DOS of Zr_xBe_{100-x} is formed by the Zr d non-bonding states. The low-energy peak in the DOS is due to bonding Be s–Zr p interactions, which increase with Be content. This explains the calculated values of the DOS at the Fermi level, which are in accordance with recent specific heat data.

Comparing our results with the $N(0)$ values extracted from low-temperature measurements, we have shown that a good agreement between theory and experiment in Ni–B and Zr–Be glasses can be achieved by taking into account the electron–phonon and exchange enhancement. The situation in Fe–B glasses is less simple because of a possible large contribution from spin fluctuations to the electronic specific heat. The overall agreement between theory and experiment demonstrates the reliability of the method in describing the shape and trends in the density of electron states in topologically disordered solids.

Finally, it is worth mentioning that the accurate description of the electron density of states of the amorphous systems we have described requires rather moderate computational efforts when the atomic spheres approximation is used in combination with the recursion method for clusters containing a few hundred atoms. The TB-LMTO method involves a few well controlled approximations which makes the results quite reliable. Further development of the RS-TB-LMTO method will allow us to gain a deeper insight into the nature of the amorphous state and to study the effects of spin polarization and the response functions in greater detail.

Acknowledgments

AMB is grateful to R Haydock, V Heine, C Nex and D Pettifor for valuable discussions about the different aspects of the recursion method and interest in the present work. AMB acknowledges enlightening discussions with O K Andersen about the TB-LMTO method. The present work was supported in part by the SERC, UK.

References

[1] Hasegawa R, O'Handley R C, Tanner L E, Ray R and Kavesh S 1976 *Appl. Phys. Lett.* **29** 219
[2] Hasegawa R and Ray R 1978 *J. Appl. Phys.* **49** 4174
[3] Bakonyi I, Pannisod P, Durand J and Hasegawa R 1984 *J. Non-Cryst. Solids* **61 & 62** 1189
[4] Bakonyi I, Ebert H, Socher W, Voitländer J, Wachtel E, Willmann N and Predel B 1987 *J. Magn. Magn. Mater.* **68** 47
[5] Burgstaller A, Socher W, Voitländer J, Bakonyi I, Tóth-Kádár E, Lovas A and Ebert H 1992 *J. Magn. Magn. Mater.* **109** 117
[6] Fukamichi K, Kikuchi M, Arakawa S and Masumoto T 1977 *Solid State Commun.* **23** 955
[7] Paul Th and Neddermeyer H 1985 *J. Phys. F: Met. Phys.* **15** 79
[8] Amamou A, Aliaga Guerra D, Panissod P, Krill G and Küntzler R 1980 *J. Physique* **41** C8 396
[9] Kiessling A 1950 *Acta Chem. Scand.* 4 146, 209
[10] Ishmaev S N, Isakov S L, Sadikov I P, Svab E, Koszegi S, Lovas A and Meszaros Gy 1987 *J. Non-Cryst. Solids* **94** 11
[11] Gardner P P, Cowlam N and Davies H A 1985 *J. Phys. F: Met. Phys.* **15** 769
[12] Bratkovsky A M and Smirnov A V 1990 *Phys. Lett.* **146A** 522
Bratkovsky A M and Smirnov A V 1990 *J. Non-Cryst. Solids* **117/118** 211
[13] Bratkovsky A M and Smirnov A V 1991 *J. Phys.: Condens. Matter* **3** 5153

[14] Bratkovsky A M, Isakov S L, Ishmaev S N, Sadikov I P, Smirnov A V, Syrykh G F, Hlopkin M N and Chernoplekov N A 1992 *Proc. 8th Int. Conf. on Liquid and Amorphous Metals (LAM8, Wien); J. Non-Cryst. Solids* at press; 1991 *Sov. Phys.–JETP* **73** 772
[15] Jones R O and Gunnarsson O 1989 *Rev. Mod. Phys.* **61** 689
[16] Pettifor D 1992 *Electron Theory in Alloy Design* ed D Pettifor and A Cottrell (London: The Institute of Materials) p 81
[17] Haydock R, Heine V and Kelly M J 1975 *J. Phys. C: Solid State Phys.* **8** 2591
[18] Andersen O K and Jepsen O 1984 *Phys. Rev. Lett.* **53** 2571
[19] Andersen O K 1975 *Phys. Rev.* B **12** 3060
[20] Andersen O K, Pawlowska Z and Jepsen O 1986 *Phys. Rev.* B **34** 5253
[21] Car R and Parrinello M 1984 *Phys. Rev. Lett.* **55** 2471
[22] Car R and Parrinello M 1988 *Phys. Rev. Lett.* **60**
Stich I, Car R and Parrinello M 1991 *Phys. Rev.* B **44** 11 092
[23] Pasquarello A, Laasonen K, Car R, Lee C and Vanderbilt D 1992 *Phys. Rev. Lett.* **69** 1982
[24] Vanderbilt D 1990 Phys. Rev. B **41** 7892
[25] Gaskell P H 1983 *Glassy Metals II* ed H Beck and H-J Güntherodt (Berlin: Springer)
[26] Fujiwara T, Chen H S and Waseda Y 1981 *J. Phys. F: Met. Phys.* **11** 1327
[27] Fujiwara T 1984 *J. Non-Cryst. Solids* **61 & 62** 1039
[28] Bose S K, Winer K and Andersen O K 1988 *Phys. Rev.* B **37** 6262
[29] Nowak H J, Andersen O K, Fujiwara T, Jepsen O and Vargas P 1991 *Phys. Rev.* B **44** 3577
[30] Andersen O K, Jepsen O and Sob M 1987 *Electronic Band Structure and its Applications (Springer Lecture Notes in Physics 283)* ed M Yussouff (Berlin: Springer) p 1
[31] Bratkovsky A M and Savrasov S Yu 1990 *J. Comput. Phys.* **88** 243
[32] Bratkovsky A M, Vaks V G and Trefilov A V 1983 *J. Phys. F: Met. Phys.* **13** 2517
[33] Allan G 1984 *J. Phys. C: Solid State Phys.* **17** 3945
[34] Nex C M M 1981 *Comput. Phys. Commun.* **34** 101
Nex C M M 1978 *J. Phys. A: Math. Gen.* **11** 653
[35] Beer N and Pettifor D 1984 *The Electronic Structure of Complex Systems* ed P Phariseau and W M Temmerman (New York: Plenum) p 769
[36] Bratkovsky A M, Rashkeev S N and Wendin G 1992 *Phys. Rev.* B submitted
[37] Peduto P R, Frota-Pessôa S and Methfessel M S 1991 *Phys. Rev.* B **44** 13 283
[38] Cooper J D, Gibb T C, Greenwood N N and Parish N V 1964 *Trans. Faraday Soc.* **60** 2097
[39] Brown P J and Cox J L 1971 *Phil. Mag.* **23** 705
Perkins R S and Brown P J 1974 *J. Phys. F: Met. Phys.* **4** 906
[40] Mohn P and Pettifor D G 1988 *J. Phys. C: Solid State Phys.* **21** 2829
Mohn P 1988 *J. Phys. C: Solid State Phys.* **21** 2841
[41] Andersen O K, Jepsen O and Glötzel D 1985 *Highlights of Condensed Matter Theory* ed F Bassani, F Fumi and M P Tosi (Amsterdam: North-Holland)
[42] Hiroyoshi H, Fukamichi K, Kikuchi M, Hoshi A and Masumoto T 1978 *Phys. Lett.* **65A** 163
[43] Bayreuther G, Enders G, Hoffmann H, Korndörfer U, Oesterreicher W, Röll K and Takahashi M 1983 *J. Magn. Magn. Mater.* **31–34** 1535
[44] Buschow K and van Engen P G 1981 *J. Appl. Phys.* **52** 3557
[45] Hatta S and Egami T 1979 *J. Appl. Phys.* **50** 1589
[46] Ostermeier H, Fembacher W and Krey U 1988 *Z. Phys. Chemie Neue Folge* **157** 489
[47] Bratkovsky A M and Smirnov A V 1992 *Proc. 8th Int. Conf. on Liquid and Amorphous Metals (LAM8, Wien); J. Non-Cryst. Solids* at press
[48] Aryasetiawan F 1992 *Phys. Rev.* B **46** 13 057
[49] Altounian Z, Harris R and Stroem-Olsen J O 1984 *J. Non-Cryst. Solids* **61 & 62** 1185
[50] Kuentzler R, Bakonyi I and Lovas A 1985 *Solid State Commun.* **55** 567
[51] Motsay R, Wang L Q, Onn D G, Donald I W and Davies H A 1982 *J. Appl. Phys.* **53** 7774
[52] Matsuura M, Mizutani U and Yazawa Y 1981 *J. Phys. F: Met. Phys.* **11** 1393
[53] Gelatt C D, Williams A R and Moruzzi V L 1984 *Phys. Rev.* B **29** 1620
[54] Bratkovsky A M and Smirnov A V 1993 *Phys. Rev.* B submitted